

# Parallel RF transmission in MRI

Ulrich Katscher\* and Peter Börnert

Philips Research Laboratories, Hamburg, Roentgenstr. 24–26, D-22335 Hamburg Germany

Received 7 September 2004; Revised 30 September 2005; Accepted 14 March 2006

**ABSTRACT:** Following the development of parallel imaging, parallel transmission describes the use of multiple RF transmit coils. Parallel transmission can be applied to improve RF excitation, in particular, multidimensional, spatially selective RF excitation. For instance, parallel transmission is able to shorten spatially selective RF pulses in two or three dimensions, or to minimize the occurring SAR. One potential major application might be the compensation of patient-induced  $B_1$  inhomogeneities, particularly at high main fields. This paper provides an overview of selected aspects of this new transmission approach. The basic principles of parallel transmission are discussed, initial experimental proofs are described, and the impact of error propagation on coil design for parallel transmission is outlined. Copyright © 2006 John Wiley & Sons, Ltd.

**KEYWORDS:** parallel transmission; transmit SENSE; parallel excitation; spatially selective RF pulses; multidimensional RF pulses; RF coil array design; SAR; parallel imaging

## INTRODUCTION

The introduction of multiple receive coils in the 1980s denotes an important milestone in the history of MRI (1,2). Multiple receive coils offer a degree of freedom that can be utilized in several directions. On one hand, the signal-to-noise ratio (SNR) can be improved (2) or on the other hand, as suggested in the late 1980s, multiple receive coils can be used to shorten the acquisition (3,4). This approach, nowadays called ‘parallel imaging’, can be divided into two basic techniques, named ‘simultaneous acquisition of spatial harmonics’ (‘SMASH’) (5) and ‘sensitivity encoding’ (‘SENSE’) (6). The original difference between these approaches is that the central matrix inversion present in both is performed in the Fourier domain or in the spatial domain.

Equivalent to the development of parallel imaging, multiple transmit coils could be utilized to perform ‘parallel transmission’. The young history of ‘parallel transmission’ shows some similarities to the developments in parallel imaging. With the introduction of human high field proton MR systems, problems of  $B_1$  inhomogeneities caused by dielectric resonance effects came into focus. Multiport excitation for birdcage-type coils was proposed as a measure to improve the RF homogeneity in the excited volume (7,8). The underlying hardware could thus be considered as a multielement transmit coil array, which allows independent adjustment

of the phase and amplitude of the otherwise identical waveforms for the individual ports. Meanwhile initial attempts have been made to show the basic feasibility of this concept for RF shimming (9–12).

Recently, RF pulses were suggested, which differ not only in amplitude and phase, but in the complete time-course for the individual transmit channels (13,14). This degree of freedom offers the possibility to improve spatially selective multidimensional RF pulses (15), for example, by shortening the pulse duration, enhancing their spatial definition, or reducing their required RF power. This might be useful for volume selective excitation (15,16) [e.g. for MR spectroscopy (17)] or outer volume signal suppression, for curved slice imaging (18), or for navigators employed for motion sensing (19). Furthermore, parallel transmission might ease the application of three-dimensional pulses (17,20–22), which are limited by the finite lifetime of the transverse magnetization and the main field homogeneity. Finally, the compensation of patient induced RF inhomogeneities seems to emerge as a major application of the approach (11,23,24), particularly at high main fields.

Based on the analogy between RF pulse design and MR imaging (15,25), parallel transmission applies the principles of parallel imaging to RF transmission (13,14). As in parallel imaging, the two different approaches proposed for parallel transmission differ in the central matrix inversion. Either it is performed in the Fourier space (13) or in the spatial domain (14). While the first approach is capable of supporting arbitrary trajectories in the excitation  $k$ -space, the latter is restricted to Cartesian ones.

In the present paper both parallel transmission approaches will be briefly outlined. Simulations are

\*Correspondence to: U. Katscher, Philips Research Laboratories, Roentgenstrasse 24–26, D-22335 Hamburg, Germany.  
E-mail: ulrich.katscher@philips.com

**Abbreviations used:** FOX, field of excitation; MR, magnetic resonance; MRI, magnetic resonance imaging; RF, radio frequency; SAR, specific energy absorption rate; SENSE, sensitivity encoding; TEM, transverse electromagnetic.

presented illustrating basic aspects of parallel transmission and first experimental steps are summarized. Furthermore, consequences for the error propagation will be investigated and basic considerations on coil design will be discussed.

## THEORY

In parallel MR imaging,  $k$ -space is undersampled, while data acquisition is performed with a number of individual receive coils. Thus, the central question in parallel imaging might be formulated as follows: given multiple measured, undersampled data sets from the individual coils, how does one get a single, entire image? This question has been answered so far by Sodickson *et al.* (5) and Pruessmann *et al.* (6) and numerous other authors—see other papers in this volume for references.

In the case of parallel transmission using multiple transmission coils, the analogous question could be: given a single, entire spatial excitation pattern as a target, how does one get the individual, undersampled spatial patterns for each of the individual transmit coils? In the following, the answer to the latter question will be briefly outlined. Mathematical details can be found in the corresponding literature (13,14).

Put more formally, the above-mentioned question reads: what undersampled spatial patterns  $P_i(\mathbf{x})$  have to be simultaneously excited by the  $N$  transmit coils, each exhibiting a characteristic sensitivity profile  $S_i(\mathbf{x})$ , to obtain the desired excitation pattern  $P_{des}(\mathbf{x})$ ? This leads to eqn (1), which turns out to be the central equation of parallel transmission

$$P_{des}(\mathbf{x}) = \sum_{i=1}^N S_i(\mathbf{x}) P_i(\mathbf{x}) \quad (1)$$

Here,  $P_{des}(\mathbf{x})$  is defined within the field of excitation (FOX), assumed to be discretized on  $M$  spatial pixels. The linear equation (1) states that the superposition of all the individual pulse profiles  $P_i(\mathbf{x})$ , weighted by the corresponding (complex) coil sensitivity profiles, should yield the desired excitation pattern. It is assumed, that the  $S_i(\mathbf{x})$  are known via  $B_1$  mapping techniques (26–28). If the transmit coils can be used in the receive mode as well, methods known from parallel imaging can be employed, assuming the reciprocal principle holds (6,29). To derive the unknown, wanted waveforms  $B_{1i}(t)$  for the  $N$  transmit coils from eqn (1), the following three steps have to be performed.

(1) Equation (1) has to be transformed into the Fourier domain. Thus, instead of the unknown  $P_i(\mathbf{x})$  given in eqn (1), now the equation contains the unknown  $p_i(\mathbf{k})$ :

$$P_{des}(\mathbf{k}) = \sum_{i=1}^N S_i(\mathbf{k}) \otimes p_i(\mathbf{k}) \quad (2)$$

This step is performed, since the  $B_1$  waveform to excite a desired magnetization pattern is just its Fourier

transform sampled along the chosen  $k$ -space trajectory multiplied by some trajectory-dependent weighting coefficients. This is according to Pauly's RF pulse design concept based on the small tip angle approximation (15), which can remain a useful approximation for selected excitation  $k$ -space trajectories even for higher flip angles (30).

In a slightly different formulation of eqn (2) (31), only the  $P_i(\mathbf{x})$  term in eqn (1) is transformed to Fourier domain:

$$P_{des}(\mathbf{x}) = \sum_{i=1}^N S_i(\mathbf{x}) A(\mathbf{x}, \mathbf{k}) p_i(\mathbf{k}) \quad (3)$$

where the Fourier encoding matrix  $A \approx \exp(i\mathbf{x}\mathbf{k})$  has explicitly been introduced (31). This approach can be convenient, for example to restrict the excitation pattern  $P_{des}(\mathbf{x})$  to a finite area within the FOX.

(2) To solve for the required  $p_i(\mathbf{k})$ , eqn (2) has to be 'inverted', which is a nontrivial task for the general case of an arbitrary  $k$ -space trajectory. To facilitate this, the sensitivities  $s_i(\mathbf{k})$  have to be grouped into a single, 'invertible' sensitivity matrix  $s_{full}$ , and, correspondingly, the individual  $p_i(\mathbf{k})$  to a single vector  $p_{full}$  (13):

$$P_{des}(\mathbf{k}) = s_{full}(\mathbf{k}) p_{full}(\mathbf{k}) \quad (4)$$

Then, this re-formulated equation can be solved using the pseudoinverse  $s_{full}^+$ , which is the optimal solution in the least squares sense:

$$p_{full} = s_{full}^H \left( s_{full} s_{full}^H \right)^{-1} P_{des} = s_{full}^+ P_{des} \quad (5)$$

The individual excitation patterns  $p_i(\mathbf{k})$  can be extracted from  $p_{full}$ , which represents the general solution to eqn (2) without any additional constraints. The separation of the  $p_i(\mathbf{k})$  starting from eqn (3) instead eqn (2) can be performed using a corresponding procedure.

We now consider the special case of a Cartesian, echo-planar like  $k$ -space trajectory, which is uniformly under-sampled in one dimension. In this case, in the spatial domain voxels are folded onto each other in groups with small numbers in each, which is described by the corresponding point spread function of the sampling scheme. As known from parallel imaging, this special case can be solved in the spatial domain (6) and leads to a small size of the sensitivity matrix to be inverted. This approach was chosen by Zhu (14), where the solution for the  $p_i(\mathbf{k})$  is written as an integral over the FOX:

$$p_i(\mathbf{k}) = \int_{FOX} h_i(\mathbf{x}) P_{des}(\mathbf{x}) e^{-i2\pi\mathbf{k}\mathbf{x}} d\mathbf{x} \quad (6)$$

In this equation, the  $h_i$  are derived from the inversion of a sensitivity matrix  $C[S_1(\mathbf{x}), S_2(\mathbf{x}), \dots, S_N(\mathbf{x})]$  (14). The inversion of this sensitivity matrix  $C$  is the central step of the approach and might be compared with the inversion of the matrix  $s_{full}$  [eqn (4)]. Both matrices  $s_{full}$  and  $C$  depend

solely on the spatial sensitivity distributions  $S_i$ , but differ in their detailed definition (13,14).

(3) Once the  $p_i(\mathbf{k})$  are calculated via eqn (5) or (6), the mapping  $d\mathbf{k} \rightarrow W(t)dt$  between  $\mathbf{k}$  and  $t$  according to the chosen  $k$ -space trajectory has to be performed. This yields the actual  $B_1$  waveforms applied in the time domain. The weighting function  $W(t)$  corresponds to the  $k$ -space sampling density, which is constant for Cartesian trajectories. The wanted waveforms can be calculated for each individual coil via

$$B_{1i}(t) = W(t)p_i(\mathbf{k}(t)) \quad (7)$$

The resulting degree of freedom introduced by the use of multiple transmit coils can be exploited in several directions. A major application is given by the reduction of the pulse duration by a factor  $R$ , corresponding to the reduction of acquisition time in parallel imaging. Instead of reducing the pulse duration, the spatial definition of the excitation pattern can be increased without changing the pulse duration. A further possibility is to utilize multiple transmit coils is to reduce the required RF power, and thus, the occurring specific energy absorption rate (SAR) (13,14,32). The reduction of the RF power can be demonstrated by solving eqn (4) using a modified least square error function  $\delta$ :

$$\delta = \|p_{des} - s_{full} p_{full}\|^2 + \lambda \|p_{full}\|^2 \quad (8)$$

introducing the regularization parameter  $\lambda$  (33). The first term on the right-hand side of eqn (8) accounts for the correct excitation of the desired pattern. The second term on the right hand side, i.e. the minimum norm condition, ensures that the vector  $p_{full}$  is also minimized. The norm  $\|p_{full}\|$  is proportional to the time-integrated  $B_1$  waveforms of all coils:

$$\|p_{full}\|^2 \sim \sum_{i=1}^N \int B_{1i}^2(t) dt \sim P_{RF} \quad (9)$$

which again is proportional to the RF power  $P_{RF}$  required for the corresponding excitation. Thus, solving eqn (8) replaces eqn (5) with

$$p_{full} = s_{full}^H (s_{full} s_{full}^H + \lambda)^{-1} p_{des} \quad (10)$$

which leads to  $B_1$  waveforms with  $P_{RF}$  minimized within the given experimental setup. As shown in ref. (11),  $P_{RF}$  could be taken as an estimate for the occurring SAR, defined via the electrical fields  $\vec{E}_i$  of the different transmit elements:

$$\text{SAR} \sim \left( \sum_{i=1}^N \vec{E}_i \right)^2 \quad (11)$$

Instead of minimizing the mean RF power via eqn (8), it is also possible to minimize peak values of the RF

pulses (34). This might help to circumvent restrictions arising from limited amplifier performance.

As discussed above, a different form of parallel transmission is performed in RF shimming, which is desirable especially for high field applications. Here, the amplitudes  $A_i$  and phases  $\phi_i$  of the otherwise identical  $B_1$  waveforms are adjusted for the different transmit array elements  $I$  to yield optimal spatial excitation homogeneity (7–9). The optimum  $A_i$  and  $\phi_i$  can be derived from eqn (1) if the individual excitation pattern  $P_i(\mathbf{x})$  are replaced by constant weighting factors  $F_i = A_i \exp(i\phi_i)$ . In this case, eqn (1) can be solved for the  $F_i$  via a matrix inversion in the image domain, choosing a constant  $P_{des}(\mathbf{x})$ . Also non-constant  $P_{des}(\mathbf{x})$  might be chosen in this framework. Formally, the  $F_i$  can be interpreted via eqn (2) as the asymptotic limit of spatially selective RF pulses with a pulse length reduced to only one data point, i.e.  $R = M$  (35).

## SIMULATIONS

It is important to know how sensitive the RF pulse performance is on the transmit coil array geometry. This pulse performance has been studied via electromagnetic simulation tools, modeling different experimental setups. In these studies, the transmit elements of the simulated coil arrays are assumed to be fully decoupled, to concentrate on the ideal behavior of the approach. The transmit elements are modelled using ‘typical’ sensitivity distributions, and thus represent typical examples of RF pulse performance. Moreover, simplified patient models are applied using typical electrical properties. Further details can be found in Refs (35–37).

One possible benchmark for the RF pulse performance is excitation error, defined as the root mean squared difference between desired and obtained excitation pattern. Our simulations showed that, for an array of  $N=2$  transmit elements and a time reduction of  $R=2$ , this excitation error is significantly enhanced only for very artificial cases (36). In these simulations, a transmit array of circular coils, tuned to 128 MHz, and a circular desired excitation pattern were assumed. First, the two coils were placed on top of each other, which of course leads to a divergent solution. Placing the two coils apart with a certain angular distance  $\Delta\varphi$  yielded satisfactory results for  $\Delta\varphi \geq 3-5^\circ$  (Fig. 1). For larger  $\Delta\varphi$ , no further decrease of the resulting excitation error in the simulated excitation pattern was observed (36). These simulations were extended for larger numbers of transmit elements and higher reduction factors (35). Here, parallel transmission was applied to obtain a homogeneous RF excitation inside a spherical head model simulating a TEM resonator at  $B_0 = 3$  T with up to  $N=32$  transmit elements (Fig. 2). As one might expect, the excitation error increases with increasing reduction factors. However, at least within the simplifications of this

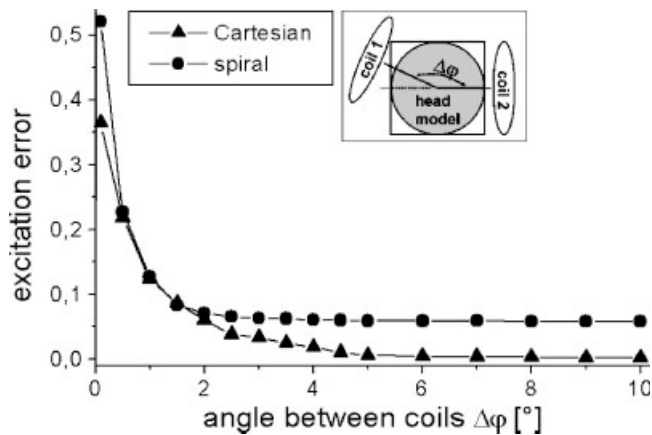


**Figure 1.** Influence of the coil array geometry on the desired circular excitation pattern (simulation scenario depicted in the inset). The excitation error, i.e. the standard deviation between desired and excited pattern, is depicted for two transmit coils and  $R=2$ . For both the Cartesian and the spiral  $k$ -space trajectory, the reconstruction error increases only for  $\Delta\phi < 2-4^\circ$ , i.e. for coils lying almost on top of each other

simulation, high reduction factors seem to be feasible, i.e. residual errors were still below the expected system noise. Figure 2 furthermore underlines that, the more coils used, the lower the excitation error. Alternatively, by accepting larger errors, it is also possible to increase the reduction factor beyond the number of transmit coils used. Such a case corresponds in parallel imaging domain to the case of ‘underdetermined SENSE’ (38). Figure 2 is based on a Cartesian  $k$ -space trajectory. Using a spiral trajectory, the excitation error shows qualitatively the same overall behavior; however, it is roughly three times higher than in the Cartesian case. This difference, which is also visible in Fig. 1, is not a feature of parallel transmission. It is caused by gridding effects between the Cartesian

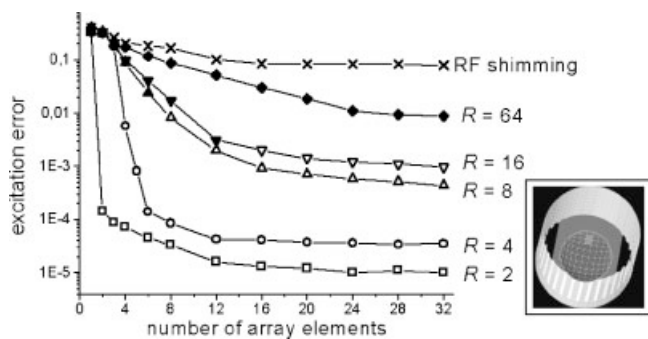


**Figure 2.** Influence of the number of transmit elements  $N$  and the reduction factor  $R$  on the excitation result for the compensation of  $B_1$  inhomogeneities at 3T (simulation scenario depicted in the inset). The excitation error, i.e. the standard deviation between desired and excited pattern, is depicted as a function of  $N$  and  $R$ . The filled symbols indicate cases  $N < R$ , the open symbols cases  $N \geq R$ . A Cartesian  $k$ -space trajectory is used. The asymptotic limit is given by adjusting amplitude and phase of each array element (‘RF shimming’)

definition of the desired excitation pattern and the non-Cartesian  $k$ -space trajectory.

When the sensitivity matrix  $s_{full}$  to be inverted becomes ill-posed, the norm of the resulting vector  $p_{full}$ , containing the RF waveforms, may increase. As discussed above, this increase would lead to an increase of the required RF power and the SAR, respectively. Thus, SAR could serve as a more stringent coil design criterion than the excitation error discussed before. This is confirmed by a simulation similar to that described above (36), where mean SAR is calculated via eqn (11) for  $N=2$  circular coils and  $R=2$ . As expected, an angular coil distance of  $\Delta\phi = 180^\circ$  yields minimal SAR, i.e. the coils should be placed on opposite sides of the patient (Fig. 3). The simulation shows that deviations of more than  $\Delta\phi \approx 45^\circ$  from the optimal position  $\Delta\phi = 180^\circ$  are necessary to cause SAR increase of more than 10% (36).

As for the excitation error discussed above, the SAR estimation via eqn (11) was repeated for the case  $R, N > 2$  to model the situation for the TEM resonator head coil described above (Fig. 4) (37). The optimal case is given if the repetition time is assumed to remain unchanged while reducing the RF pulse duration. Here, the reduction factor  $R$  has no significant impact on SAR. The worst case occurs when the repetition time is chosen to be the minimum consistent with the RF pulse duration, which leads to a roughly linear increase of SAR with  $R$ .

To summarize these findings, it seems that the RF pulse performance proves to be fairly stable, and thus, problems caused by ill-posed inversion appear to play only a minor role in parallel transmission. This allows greater freedom in the design of coil arrays for parallel transmission than for parallel imaging. On the other hand, since only ‘typical’ example coils have been used for these simulations, the development of dedicated transmit arrays may turn out to stabilize the RF pulse performance even further.

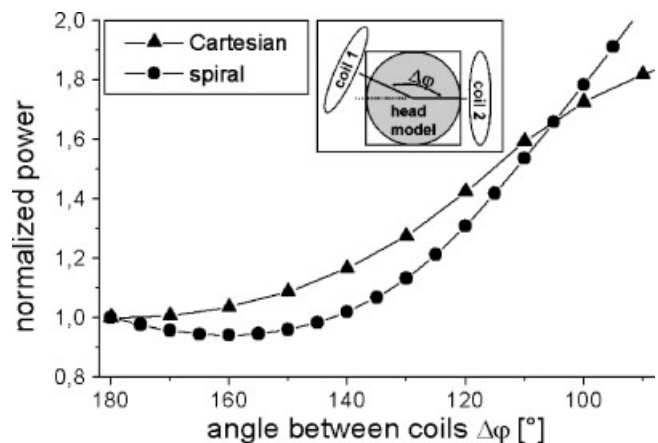


**Figure 3.** Influence of the coil array geometry on required RF power (simulation scenario depicted in the inset). Two transmit coils and a reduction factor  $R=2$  are assumed. Decreasing the angle between the coils from  $\Delta\phi = 180^\circ$  to  $\Delta\phi = 130^\circ$  enhances the required RF power by roughly 20% for both trajectories regarded

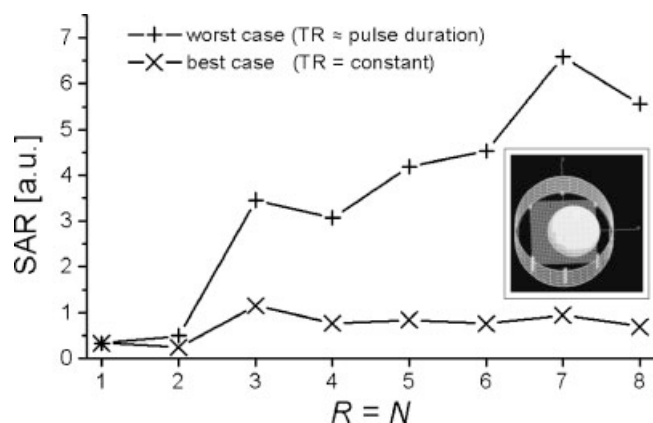


**Figure 4.** SAR simulated for an eight-channel TEM resonator head coil (simulation scenario depicted in the inset). The SAR is calculated assuming a Cartesian trajectory and a reduction factor  $R$  equal the number of transmit elements  $N$ . If TR is kept constant, the fraction of the RF pulse duration decreases with increasing  $R$ . Here, the resulting simulated SAR is in first order independent of  $R$ . In the worst case, TR is chosen to be hardly longer than the RF pulse duration. The simulation yields a roughly linear increase of SAR in  $R$

## EXPERIMENTS

The theoretical development of parallel transmission preceded practical capabilities for experimental tests by several years. Lack of suitable MR systems required experimental confirmation of parallel transmission to be realized using work-arounds (13,14). To mimic scanning with different transmit coils, experiments were broken down into separate sub-experiments each using a different RF excitation waveform and transmit coil. In these separate sub-experiments, the RF pulse profiles have been measured for the different  $B_1$  waveforms and added afterwards (Fig. 5). This final superposition was equivalent to a single experiment transmitting all RF pulses simultaneously, provided the small tip angle approximation can be applied.

In parallel to these experiments, multielement-transmit coils were being developed (39–41) in preparation for truly multichannel MR systems. In the next step, parallel transmission was performed using genuinely simultaneous RF pulses, differing, however, only in the overall amplitude and phase (9–12). This setup allowed reduction of RF inhomogeneities, confirming predictions of previous simulations (8).

Then, two groups demonstrated prototype MR systems capable of parallel multidimensional pulses (12,42). In one case, four 1.5 T spectrometers (EXCITE II/General Electric Health Care, USA) were combined to drive an eight-channel head coil and a six-channel planar surface coil (42). A master/slave mode was implemented, synchronizing all transmit channels at a nanosecond level. The  $B_1$  maps were acquired similar to the technique described in Ref. (6). In this framework, a rectangular

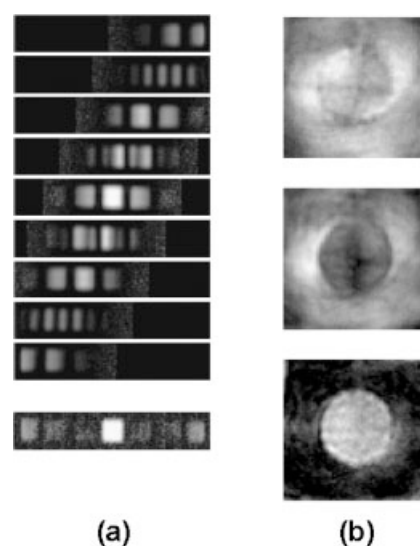


**Figure 5.** Early parallel transmission experiments using successive single-channel excitations. (a) Results using a planar array of nine coils and a reduction factor of  $R=4$ . The first nine lines show the individual patterns excited by the individual elements of the transmit array. The bottom line shows the resulting superposition of the individual excitation patterns yielding the desired rectangular pattern in the center of the FOX (14). (b) Results using two transmit setups and a reduction factor of  $R=2$ . The two upper images show the individual excitation patterns measured for the two different coil sensitivities employed. The lower image shows the resulting superposition of the individual excitation patterns yielding the desired circular pattern (13). In both approaches, the aliasing artifacts visible in the individual excitation patterns in the upper rows are reduced significantly in the final result shown in the bottom row

pattern, discretized on a  $32 \times 32$  grid, was excited using a reduction factor  $R=4$ . The accuracy of the pattern reproduction was above 90%. The approach was also applied to RF shimming (11).

Simultaneously, experiments were presented from a 4.7 T system (BioSpec/Bruker BioSpin MRI, Germany) (12). This system was equipped with an  $N=3$  channel current-sheet-antenna array integrated into a birdcage-type resonator owning a homogeneous transmit profile. A checkerboard target pattern was excited using a modified spin-echo sequence with a two-dimensional spatially selective excitation and slice selective refocusing. The result for the unreduced case  $R=1$ , i.e. using a spiral  $k$ -space trajectory with 16 revolutions and the resonator, is shown in Fig. 6(a). Using the three-channel system, reduction factors  $R=2$  and  $R=2.67$  were realized, i.e. a spiral  $k$ -space trajectory with eight and six revolutions, respectively [Fig. 6(b and c)]. Only minor image quality degradation was observed for these cases: the corresponding correlations decreased by less than 1%. Instead, under off-resonance and  $B_0$  inhomogeneity conditions, results of parallel transmission clearly outperform the unreduced case. Here, an increase of the correlation of up to 20% has been observed (12).

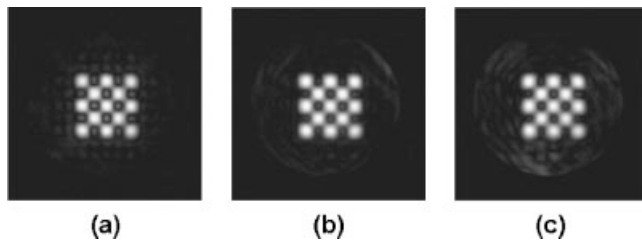


**Figure 6.** Experimental results from a 4.7T system equipped with a  $N=3$  channel transmit array integrated into a birdcage-type resonator with a homogeneous transmit profile (12). (a) Result for the unreduced case ( $R=N=1$ ) using the resonator. (b) Result for the reduction factor  $R=2$  using the  $N=3$  channel system. (c) Result for the reduction factor  $R=2.67$  using the  $N=3$  channel system

## DISCUSSION

The concept of parallel transmission was developed to improve multidimensional RF pulses. After numerous theoretical investigations and numerical simulations in this field, the first experimental steps were taken to prove the basic feasibility of parallel transmission. Work is now starting on practical systems that will allow parallel transmit to be fully tested and clinical applications developed as we move towards parallel transmit being a standard feature of modern high-field MR systems. Several issues warrant further consideration as follows.

Noise in parallel transmission might originate from, for example, the D/A converting process and RF amplifier imperfections. This system noise affects the individual pulse profiles  $P_l(\mathbf{x})$ , and thus influences the final result in a linear way as a superposition in the spatial domain [cf. eqn (1)]. Errors in the coil sensitivity profiles caused by noise or measurement imperfections also influence the final resulting linearly via eqn (1). It is important to note that the system noise does not interact with the central matrix inversion [eqn (5)]. This is a crucial difference with respect to parallel imaging, where the system noise generated in the receive chain is enhanced, if the matrix inversion is ill-conditioned (6). In parallel imaging, the inverted matrix is multiplied by the measured data bearing noise. In parallel transmission, the inverted matrix is multiplied by the desired excitation pattern, which is free from noise (Fig. 7). In that respect, the concept of the geometry factor as deduced for parallel imaging (6) cannot be adapted directly to parallel transmission.

If the inverse problem of parallel transmission is ill-posed, the superposition of eqn (1) does not lead to a complete cancellation of the subsampling artifacts, and noise-like aliasing structures appear in the final result. The problem becomes ill-posed if the spatial frequency components of the actual coil sensitivity profiles are not able to compensate for the missing parts of a reduced  $k$ -space trajectory. Thus, a proper interplay between the coil sensitivity profiles and the involved trajectories has to be

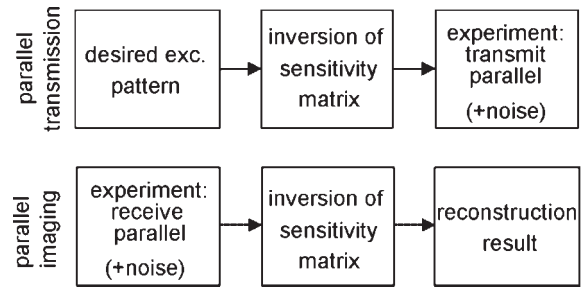


**Figure 7.** Schematic comparison of parallel transmission and imaging. Experimental noise comes into play after/before the inversion of the sensitivity matrix, which leads to a larger robustness of parallel transmission than parallel imaging

found. From this interplay, conditions for the sensitivity profiles, and thus, the used coil array can be derived.

Parallel transmission is not simply the reciprocal of the parallel acquisition case. Both parallel transmission and imaging are a combination of a forward and an inverse matrix problem. Neither the front end of the MR system (i.e. the coil array) nor the spin system of the patient's body is able to invert a matrix. However, the scanner can superimpose all kinds of magnetic fields to act on the magnetization, which is equivalent to solving a forward problem. The inverse problem has to be solved on the host computer (i.e. the back end of the MR system). The data flows from back end to front end for parallel transmission and vice versa for parallel imaging. However, where the inverse problem is solved, it cannot be shifted from the back end to the front end. The inverse problem must be solved on the back end of the MR system, irrespective of the direction of the data flow. This might explain why parallel transmission cannot be derived by simply inverting the parallel imaging algorithm.

Comparing the time reduction factor  $R$  with the number of available transmit coils  $N$ , the three cases  $R=N$ ,  $R < N$ , and  $R > N$  can be distinguished. In parallel imaging, first the more obvious cases  $R \leq N$  have been studied (6). Later it was shown, that parallel imaging is also possible using  $R > N$ , if  $R$  is chosen within certain limits (38). In parallel imaging,  $R < N$  defines an overdetermined and  $R > N$  an underdetermined set of equations. Regarding parallel transmission, corresponding scenarios of  $R$  and  $N$  can be defined. However, in the mathematical framework, the case  $R > N$  now defines an overdetermined set of equation and vice versa. For instance, it is assumed that the desired magnetization pattern to be excited in the FOV is discretized on  $M$  spatial points, which enter the calculation. From these data, the waveforms for the  $N$  coils are derived, each consisting of  $M/R$  data points. Thus, the number of data points  $N \cdot M/R$  to be derived is smaller than the number  $M$  of input data points, if  $R > N$ , leading to an overdetermined scenario in opposite to parallel imaging. A further difference between parallel imaging and parallel transmission is given by the

available *a priori* knowledge, i.e. a suitable estimation of the expected result. This *a priori* knowledge can be used to stabilize the inverse problem by minimizing the distance between calculated and expected result [cf. eqn (8)], particularly for underdetermined cases. In parallel imaging, any estimations of the final anatomic image can serve as *a priori* knowledge. In parallel transmission, the expected result is not the reconstructed image, but the  $B_1$  waveforms of the individual coils. The estimation of  $B_1$  waveforms is a non-trivial task, and only zero  $B_1$  waveforms have been applied as *a priori* knowledge for cases  $R > N$  in the literature (35). Figure 2 shows the principle feasibility of this scenario, which for the limit  $R \gg N$  coincides with the 'classic' RF shimming via multiport excitation (8).

A couple of approaches for compensating system imperfections have been developed for spatially selective RF pulses, e.g.  $B_0$  inhomogeneities, imperfections in the excitation  $k$ -space trajectory or concomitant gradients (25). It might be emphasized, that these approaches are also applicable for parallelly transmitted, spatially selective RF pulses (31). Similarly, other measures for RF pulse optimization might be carried forward to parallel transmission, e.g., the impact of the  $k$ -space trajectory on the occurring SAR (43) or designing three-dimensional trajectories exciting slices with a sharp profile and a low resolution in-plane homogeneity correction (44).

## SUMMARY

Parallel transmission follows the development of parallel imaging. Parallel transmission can be used to shorten the duration of spatially selective RF pulses or to increase their spatial resolution definition while maintaining the pulse duration. Other potential applications could include the reduction of the required RF power, i.e. the SAR, or RF shimming. Since parallel transmission is not just the reciprocal version of parallel imaging, the error propagation in parallel transmission does not lead to pronounced nonlinear effects as observed in parallel imaging, described by the geometry factor.

First prototypes of MR systems fully capable of parallel transmission have recently been presented. Initial experiments confirmed the feasibility of the approach, and further studies for an enhanced understanding of parallel transmission will follow. Very likely, future standard high-field MR systems will be capable of parallel transmission. These MR systems will be able to improve RF pulses in many respects, thus opening a wide range of new and exciting applications.

## REFERENCES

- Hyde JS, Jesmanowicz A, Froncisz W, Kneeland JC, Grist TM. Parallel image acquisition from noninteracting local coils. *J. Magn. Reson.* 1986; **70**: 512–517.
- Roemer PB, Edelstein WA, Hayes CE, Souza SP, Mueller OM. The NMR phased array. *Magn. Reson. Med.* 1990; **16**: 192–225.
- Carlson JW. An algorithm for NMR imaging reconstruction based on multiple RF receiver coils. *J. Magn. Reson.* 1987; **74**: 376–380.
- Hutchinson MU, Raff U. Fast MRI data acquisition using multiple detectors. *Magn. Reson. Med.* 1988; **6**: 87–91.
- Sodickson DK, Manning WJ. Simultaneous acquisition of spatial harmonics (SMASH): fast imaging with radiofrequency coil arrays. *Magn. Reson. Med.* 1997; **38**: 591–603.
- Pruessmann KP, Weiger M, Scheidegger MB, Boesiger P. SENSE: sensitivity encoding for fast MRI. *Magn. Reson. Med.* 1999; **42**: 952–962.
- Sotgiu A, Hyde JS. High-order coils as transmitters for NMR imaging. *Magn. Reson. Med.* 1986; **3**: 55–62.
- Ibrahim TS, Lee R, Baertlein BA, Kangarlu A, Robitaille PL. Application of finite difference time domain method for the design of birdcage RF head coils using multiport excitations. *Magn. Reson. Med.* 2000; **18**: 733–742.
- Seifert F, Rinneberg H. Adaptive coil control: SNR optimization of a TR volume coil for single voxel MRS at 3 T. *Proc. Int. Soc. Magn. Reson. Med.* 2002; **10**: 162.
- Adriani G, Van de Moortele PF, Wiesinger F, Moeller S, Strupp JP, Andersen P, Snyder C, Zhang X, Chen W, Pruessmann KP, Boesiger P, Vaughan T, Ugurbil K. Transmit and receive transmission line arrays for 7 Tesla parallel imaging. *Magn. Reson. Med.* 2005; **53**: 434–445.
- Zhu Y, Giaquinto R. Improving flip angle uniformity with parallel excitation. *Proc. Int. Soc. Magn. Reson. Med.* 2005; **13**: 2752.
- Ullmann P, Junge S, Wick M, Seifert F, Ruhm W, Hennig J. Experimental analysis of parallel excitation using dedicated coil setups and simultaneous RF transmission on multiple channels. *Magn. Reson. Med.* 2005; **54**: 994–1001.
- Katscher U, Börnert P, Leussler C, van den Brink J. Transmit SENSE. *Magn. Reson. Med.* 2003; **49**: 144–150.
- Zhu Y. Parallel excitation with an array of transmit coils. *Magn. Reson. Med.* 2004; **51**: 775–784.
- Pauly J, Nishimura D, Macovski A. A  $k$ -space analysis of small-tip-angle excitation. *J. Magn. Reson.* 1989; **81**: 43–56.
- Hardy VJ, Cline HE. Spatial localization in two dimensions using NMR designer pulses. *J. Magn. Reson.* 1989; **82**: 647–654.
- Bottomley PA, Hardy CJ. Progress in efficient 3-dimensional spatially localized in vivo P-31 NMR-spectroscopy using multi-dimensional spatially selective (Rho) pulses. *J. Magn. Reson.* 1987; **74**: 550–556.
- Börnert P, Schäffter T. Curved slice imaging. *Magn. Reson. Med.* 1996; **36**: 932–939.
- Sachs TS, Meyer CH, Hu BS, Kohli J, Nishimura D, Macovski A. Real-time motion detection in spiral MRI using navigators. *Magn. Reson. Med.* 1994; **32**: 639–645.
- Pauly JM, Hu BS, Wang SJ, Nishimura DG, Macovski A. A three-dimensional spin-echo or inversion pulse. *Magn. Reson. Med.* 1993; **29**: 2–6.
- Wong ST, Roos MS. A strategy for sampling on a sphere applied to 3D selective RF pulse design. *Magn. Reson. Med.* 1994; **32**: 778–784.
- Yang GZ, Gatehouse PD, Keegan J, Mohiaddin RH, Firmin DN. Three-dimensional coronary MR angiography using zonal echo planar imaging. *Magn. Reson. Med.* 1998; **39**: 833–842.
- Saekho S, Boada FE, Noll DC, Stenger VA. Small tip angle three-dimensional tailored radiofrequency slab-select pulse for reduced B1 inhomogeneity at 3 T. *Magn. Reson. Med.* 2005; **53**: 479–484.
- Ulloa JL, Irrarrazaval P, Hajnal JV. Exploring 3D RF shimming for slice selective imaging. *Proc. Int. Soc. Mag. Reson. Med.* 2005; **13**: 21.
- Börnert P, Aldefeld B. On spatially selective RF excitation and its analogy with spiral MR image acquisition. *MAGMA* 1998; **7**: 166–178.
- Glover GH, Hayes CE, Pelc NJ, Edelstein WA, Mueller OM, Hart HR, Hardy CJ, O'Donnell M, Barber WD. Comparison of linear and circular polarization for magnetic resonance imaging. *J. Magn. Reson.* 1985; **64**: 255–270.
- Barker GJ, Simmons A, Arridge SR, Tofts PS. A simple method for investigating the effects of non-uniformity of radiofrequency transmission and radiofrequency reception in MRI. *Br. J. Radiol.* 1998; **71**: 59–67.

28. Griswold MA, Kannengiesser S, Müller M, Jakob PM. Autocalibrated accelerated parallel excitation (transmit-GRAPPA). *Proc. Int. Soc. Magn. Reson. Med.* 2005; **13**: 2435.
29. Carlsen IC, Jensen D. Reconstruction algorithm for images obtained with multi-element synergy coils. *Proc. Soc. Magn. Reson.* 1994; **2**: 834.
30. Pauly J, Nishimura D, Macovski A. A linear class of large-tip-angle selective excitation pulses. *J. Magn. Reson.* 1989; **82**: 571–587.
31. Grissom WA, Yip CY, Noll DC. An image domain approach for the design of RF pulses in transmit SENSE. *Proc. Int. Soc. Magn. Reson. Med.* 2005; **13**: 19.
32. Graesslin I, Niemann M, Harvey P, Vernickel P, Katscher U. SAR and RF power reduction with parallel excitation using non-cartesian trajectories. *MAGMA* 2005; **18**: S251.
33. Katscher U, Börnert P, van den Brink JS. Theoretical and numerical aspects of transmit SENSE. *IEEE Trans. Med. Imag.* 2004; **23**: 520–525.
34. Yip CY, Fessler JA, Noll DC. Iterative RF pulse design for multidimensional, small-tip-angle selective excitation. *Magn. Reson. Med.* 2005; **54**: 908–917.
35. Katscher U, Vernickel P, Hanft M. Static and dynamic RF-shimming in the framework of transmit SENSE. *Proc. Int. Soc. Magn. Reson. Med.* 2005; **13**: 2256.
36. Katscher U, Röhrs J, Börnert P. Basic considerations on the impact of the coil array on the performance of transmit SENSE. *MAGMA* 2005; **18**: 81–88.
37. Katscher U, Vernickel P, Overweg J. Basics of RF power behaviour in parallel transmission. *Proc. Int. Soc. Magn. Reson. Med.* 2005; **13**: 17.
38. Katscher U, Manke D. Underdetermined SENSE using a-priori knowledge. *Proc. Int. Soc. Magn. Reson. Med.* 2002; **10**: 2396.
39. Boskamp E, Lee RF. Whole body LPSA tranceive array. *Proc. Int. Soc. Magn. Reson. Med.* 2002; **10**: 903.
40. Weyers D, Boskamp E. An 8 channel volume transmit coil. *Proc. Int. Soc. Magn. Reson. Med.* 2002; **10**: 901.
41. Lee RF, Giaquinto RO, Hardy CJ. Coupling and decoupling theory and its application to the MRI phased array. *Magn. Reson. Med.* 2002; **48**: 203–213.
42. Zhu Y, Watkins R, Giaquinto R, Hardy C, Kenwood G, Mathias S, Valent T, Denzin M, Hopkins J, Peterson W, Mock B. Parallel excitation on an eight transmit-channel MRI system. *Proc. Int. Soc. Magn. Reson. Med.* 2005; **13**: 14.
43. Conolly S, Nishimura DG, Macovski A, Glover G. Variable-rate selective excitation. *J. Magn. Reson.* 1988; **78**: 440–458.
44. Yip CY, Fessler JA, Noll DC. A novel, fast and adaptive trajectory in three-dimensional excitation  $k$ -space. *Proc. Int. Soc. Magn. Reson. Med.* 2005; **13**: 2350.